Combination of searches for invisible decays of the Higgs boson using 139 fb^{-1} of proton-proton collision data at $\sqrt{s}$ = 13 TeV collected with the ATLAS experiment

The ATLAS Collaboration

Many extensions of the Standard Model predict the production of dark matter particles at the LHC. Sufficiently light dark matter particles may be produced in decays of the Higgs boson that would appear invisible to the detector. This Letter presents a statistical combination of searches for $H \rightarrow$ invisible decays where multiple production modes of the Standard Model Higgs boson are considered. These searches are performed with the ATLAS detector using 139 fb^{-1} of proton–proton collisions at a centre–of–mass energy of $\sqrt{s}$ = 13 TeV at the LHC. In combination with the results at $\sqrt{s}$ = 7 TeV and 8 TeV, an upper limit on the $H \rightarrow$ invisible branching ratio of 0.107 (0.077) at the 95% confidence level is observed (expected). These results are also interpreted in the context of models where the 125 GeV Higgs boson acts as a portal to dark matter, and limits are set on the scattering cross-section of weakly interacting massive particles and nucleons.

arXiv:2301.10731v1 [hep-ex] 25 Jan 2023

Contents

1 Introduction

Compelling astrophysical evidence suggests that dark matter (DM) comprises most of the matter in the universe [1–4]. However, its nature is still unknown and poses one of the central questions in modern physics. A possible candidate for DM is a massive, stable and electrically neutral particle χ, interacting weakly with the known particles of the Standard Model (SM).

Several theoretical frameworks predict the production of DM particles in proton–proton collisions at the Large Hadron Collider (LHC) [5–7]. In a wide class of those models, the 125 GeV Higgs boson [8, 9] acts as a portal between a dark sector and the SM sector, either through Yukawa-type couplings to fermionic DM, or other mechanisms [10–23]. If kinematically allowed, pairs of DM particles can then be produced via the decay of the Higgs boson. The DM particles would traverse the detector without interacting and are inferred indirectly through the presence of missing transverse momentum (E_T^{miss})[1] in the interaction. This additional decay channel is therefore called "invisible." In the SM, the branching fraction to invisible final states is about 0.1% [24] arising from the decay of the Higgs boson via $ZZ^* \to 4\nu$.

Direct searches for invisible decays of the Higgs boson were carried out with the ATLAS detector [25, 26] during Run 1 of the LHC, using up to 4.7 fb^{-1} of pp collision data at a centre-of-mass energy of $\sqrt{s} = 7$ TeV and up to 20.3 fb^{-1} at 8 TeV. Various event topologies were considered: vector boson fusion (VBF) [27], production in association with a Z boson (ZH) that decays into a pair of electrons or muons [28], and with a

---

[1] ATLAS uses a right-handed coordinate system with its origin at the nominal interaction point (IP) in the centre of the detector and the z-axis along the beam pipe. The x-axis points to the centre of the LHC ring, and the y-axis points upward. Cylindrical coordinates (r, ϕ) are used in the transverse plane, ϕ being the azimuthal angle around the z-axis. The pseudorapidity is defined in terms of the polar angle θ as $\eta = -\ln\tan(\theta/2)$. The distance between two objects in η–ϕ space is $\Delta R = \sqrt{(\Delta\eta)^2 + (\Delta\phi)^2}$. Transverse momentum is defined by $p_T = p\sin\theta$.

W or *Z* boson that decays into hadrons [29]. A statistical combination of these ATLAS searches resulted in an observed (expected) upper limit at the 95% confidence level (CL) on the invisible Higgs boson branching ratio of $\mathcal{B}_{H\to\text{inv}} < 0.25$ $(0.27^{+0.10}_{-0.08})$ [30]. These searches were expanded with up to 36 fb^{-1} of Run 2 data and their combination, including Run 1 results, yielding an upper limit of $\mathcal{B}_{H\to\text{inv}} < 0.26$ $(0.17^{+0.07}_{-0.05})$ at the 95% CL [31]. A combination from the CMS experiment using a similar dataset reported an observed (expected) upper limit of 0.19 (0.15) [32].

More recently, new direct searches for invisible decays of the Higgs boson using the full Run 2 data of up to 139 fb^{-1} were performed, covering most of the Higgs boson production modes, by ATLAS [33–37] and CMS [38–40]. In both experiment the VBF final state is the most sensitive channel resulting in an upper limit of 0.145 (0.103) for ATLAS and 0.18 (0.12) for CMS.

A partial combination of the ATLAS VBF and *ZH* searches together with the analyses targeting visible decays of the Higgs boson was carried out [41] and its results reduce the observed (expected) upper limit on $\mathcal{B}_{H\to\text{inv}}$ to 0.13 (0.08). Such a combination considers the impact of $\mathcal{B}_{H\to\text{inv}}$ on the Higgs boson total decay width and simultaneously determines $\mathcal{B}_{H\to\text{inv}}$, together with the coupling of the Higgs boson to all the SM particles as well as a potential contribution to undetected Higgs boson decays not generating missing transverse energy. The approach relies on a different set of assumptions to what is used in this letter.

This letter presents the statistical combination of all ATLAS direct searches for invisible decays of the Higgs boson using the full Run2 dataset. This includes the gluon–gluon fusion, VBF, *ZH* and *ttH* production modes, represented in Figure 1 and assumes the production cross-sections of the Higgs boson does not deviate from the SM predictions [24, 42–47]. In addition, a statistical combination with the combined Run 1 result [30] from ATLAS is included, yielding the most sensitive direct constraint to invisible Higgs boson decays in ATLAS.
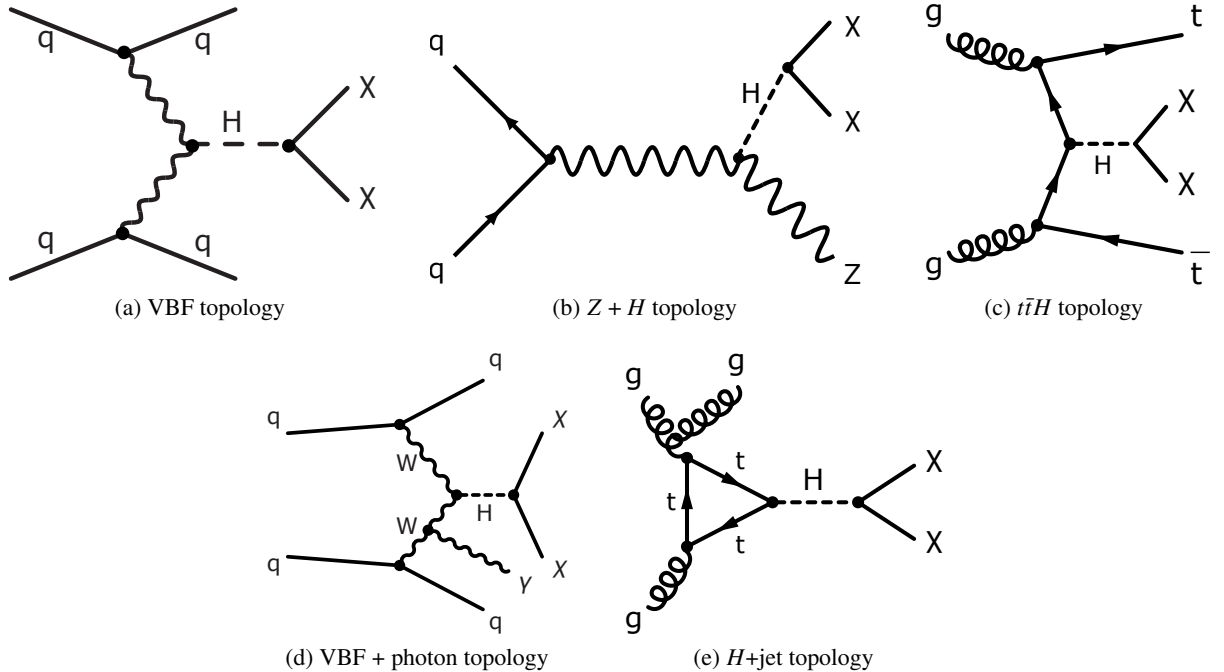

Figure 1: Diagrams illustrating the Higgs boson production mode targetted for the Run 2 searches.

2 Combination inputs

The inputs to the combination for the Run 2 result consist of searches for invisible decays of the Higgs boson, with the following production modes:

- VBF topology (VBF + E_T^{miss}) [33]

- associated production with a Z boson decaying into electrons or muons ($Z(\rightarrow \ell\ell) + E_T^{miss}$) [36]

- associated production with a $t\bar{t}$ pair, using all top-quark decay modes except those with hadronically decaying τ–leptons ($t\bar{t} + E_T^{miss}$) [48]

- VBF topology in association with an emitted photon (VBF + E_T^{miss} + γ) [34]

- gluon–gluon fusion, in association with a high p_T jet (Jet + E_T^{miss}) [37]

all of which use the full data sample, corresponding to an integrated luminosity of 139 fb^{-1}.

These analyses target different production modes of the Higgs boson and so their event selection criteria are made to be largely orthogonal by using different requirements on lepton, photon, jet and b-tagged jet multiplicity. The level of residual non-orthogonality was evaluated by considering both the data events and signal samples for all the Higgs boson production modes. The largest set of shared events is between the Jet + E_T^{miss} and VBF + E_T^{miss} searches, which select events with large missing transverse energy, no reconstructed leptons, and multiple jets in the final state. The number of overlapping events corresponds to 0.2% (1.5%) of the total data (expected signal Monte Carlo (MC) samples) events selected by the Jet + E_T^{miss} analysis. The impact of the overlap on the final combined result is negligible, altering the upper limit on $\mathcal{B}_{H\rightarrow inv}$ by less than 0.001. A brief overview of the Run 2 analyses and the inputs to the Run 1 combined result [30] is given below.

2.1 VBF + E_T^{miss} search

In the VBF production mode, the $H \rightarrow$ invisible signal is characterised by two jets with a large separation in pseudorapidity and missing transverse momentum arising from the invisible decays of the Higgs boson. The analysis targetting this signature selects events collected with a trigger selection based on the presence of E_T^{miss}. Events are further selected if their two jets with the highest p_T fulfill the VBF topology requirements: lying in opposite longitudinal hemispheres, being well separated in η, and not back-to-back in the transverse plane. In order to reduce the contribution from W, Z+jets and $t\bar{t}$ production, and to ensure orthogonality with the other analyses, events containing lepton or photon candidates and two or more jets identified as b-tagged jets [49] are vetoed.

In this signature, the dominant background sources are $Z(\rightarrow \nu\nu)$ + jets and $W(\rightarrow \ell\nu)$ + jets production, where in the latter process the charged lepton ℓ is not detected or mis-identified. These backgrounds are evaluated simultaneously using high-statistics control regions in the 1-lepton and 2-leptons channels. Such extrapolation is made possible due to the use of a dedicated theoretical calculation at next-to-leading order in the phase space that is relevant for this analysis [50]. The multijet background is directly estimated from data.

The final discrimination is obtained by splitting signal and control region events into 16 bins based on E_T^{miss}, the invariant mass of selected dijet pair, their separation in ϕ, and jet multiplicity to maximise the

signal/background separation. Assuming the SM cross-section for the VBF production mode, an observed (expected) upper limit of 0.145 (0.103) at the 95% CL is placed on $\mathcal{B}_{H\rightarrow\text{inv}}$.

2.2 $Z(\rightarrow \ell\ell) + E_\text{T}^\text{miss}$ search

The search targeting the Higgs boson production in association with a Z boson selects events containing a pair of electrons or muons and significant missing transverse momentum. The two charged leptons are required to have an invariant mass within a narrow window around the Z boson mass for the events to satisfy the signal selection requirements.

The dominant backgrounds for this signature are ZZ, where one of the Z bosons decays into a neutrino–antineutrino pair, and WZ production. Contributions from $t\bar{t}$ and WW production are estimated from data, using events with two identified different-flavour charged leptons (electrons and muons).

Beyond the signature selections, sensitivity for the $H \rightarrow$ invisible model is enhanced using a boosted decision tree (BDT) discriminator to improve the separation between signal and background. A profile likelihood fit to the BDT output distribution results in an observed (expected) upper limit on $\mathcal{B}_{H\rightarrow\text{inv}}$ of 0.185 (0.185) at the 95% CL, assuming the SM production cross-section for this process.

2.3 $t\bar{t} + E_\text{T}^\text{miss}$ search

The production mode of the Higgs boson in association with a top-quark pair is targetted by reinterpreting the combination of several searches for new phenomena in association with heavy flavour quarks [51–53]. The final states arising from this production mode are characterised by the presence of b-tagged jets and different charged lepton multiplicities, depending on the decay mode of the two W bosons from the $t\bar{t}$ decays. In addition, a relevant amount of E_T^miss is present, coming from the invisible decay products of the Higgs boson and from neutrinos.

A targetted event selection is developed for each lepton multiplicity, resulting in different dominant background contributions from SM processes: $t\bar{t}$ and $Z(\rightarrow \nu\nu)$ + jets in the 0-lepton channel, $t\bar{t}$ in the 1-lepton channel and ttZ in the 2-lepton channel. For all the combined analyses, background-enriched selections are defined in order to allow the data to aid in estimating the dominant backgrounds, and validation regions are used to verify the robustness of these estimates.

The combination of the three analyses of each lepton multiplicity, considered in this document as a single combined analysis, places an observed (expected) upper limit on $\mathcal{B}_{H\rightarrow\text{inv}}$ of 0.376 (0.295) at the 95% CL, assuming the SM production cross-section for this process.

2.4 VBF + $E_\text{T}^\text{miss} + \gamma$ search

The VBF topology is further investigated by a dedicated analysis targeting the final states with an emitted photon. The event signature is characterised by significant missing transverse momentum and one photon in the final state, in addition to a pair of forward jets. In the SM this topology can arise from $V\gamma$+jets production, where V is either a Z boson decaying into a neutrino pair or a W boson decaying leptonically, where the charged lepton is missed.
A dense neural network (DNN) was designed and trained to separate such backgrounds from the

$H \rightarrow$ invisible signal by using kinematic properties of the events. The residual SM contribution to the signal regions is estimated with the aid of specific control regions requiring the presence of electron or muon candidates, to set the normalisation of the MC simulation for $V\gamma$+jets processes. Assuming the SM production cross-section on the signal model, an observed (expected) upper limit on $\mathcal{B}_{H\rightarrow\text{inv}}$ of 0.375 (0.346) at the 95% CL is evaluated.

2.5 Jet + E_T^miss search

The gluon–gluon fusion production mode of the Higgs boson is targetted by a search for new phenomena in events with at least one jet and large missing transverse momentum. Data are collected with a trigger selection based on the presence of E_T^miss and events are vetoed if any charged lepton or photon is reconstructed.

The dominant SM background for this search arises from the irreducible process $Z \rightarrow \nu\nu$ or $W \rightarrow \ell\nu$ in association with jets, where the W boson decays into either hadronically decaying τ-leptons or undetected electrons or muons. Additional contributions include $t\bar{t}$ pair or single-top production, diboson production, and non-collision and multijet backgrounds. The estimate of the major SM processes in the analysis selection is based on a profile likelihood fit to the distribution of the p_T of the system recoiling against the jets reconstructed in the event, performed simultaneously in the signal region and in orthogonal control regions enriched with the targetted backgrounds. Assuming the SM cross-section for Higgs boson gluon–gluon fusion production, an observed (expected) upper limit on $\mathcal{B}_{H\rightarrow\text{inv}}$ of 0.329 (0.383) at the 95% CL is achieved.

2.6 Run 1 combination

The Run 1 ATLAS $H \rightarrow$ invisible combination utilises 4.7 fb^{-1} of pp collision data at $\sqrt{s} = 7$ TeV and 20.3 fb^{-1} at $\sqrt{s} = 8$ TeV [30]. This combination considers inputs from direct detection of $H \rightarrow$ invisible through Higgs bosons produced via VBF or in association with a vector boson V, where the vector boson decays either leptonically ($Z \rightarrow \ell\ell$) or hadronically ($W/Z \rightarrow jj$). All of the signal and control regions are utilized in a maximum-likelihood fit resulting in an observed (expected) upper limit of $\mathcal{B}_{H\rightarrow\text{inv}}$ < 0.252 (0.265) at the 95% CL. The sensitivity is driven by the VBF channel.

3 Statistical Model

The statistical combination of the analyses is performed by constructing the product of their respective likelihoods and maximising the resulting profile likelihood ratio [54]:

$$\Lambda(\beta; \theta) = \frac{L\left(\beta, \hat{\hat{\theta}}(\beta)\right)}{L\left(\hat{\beta}, \hat{\theta}\right)}$$

where β and θ are the parameter of interest and the nuisance parameters. In the numerator, the nuisance parameters are set to their fitted values $\hat{\hat{\theta}}(\beta)$, which maximise the likelihood function for fixed values of the parameter of interest, β. In the denominator, both the parameter of interest and the nuisance parameters are set to the values $\hat{\beta}$ and $\hat{\theta}$ which jointly maximise the likelihood. This is done following the implementation

described in Ref. [55, 56], with $\mathcal{B}_{H\to\text{inv}}$ as the parameter of interest, β. Systematic uncertainties are modelled in the likelihood function as nuisance parameters, θ, constrained by Gaussian or log-normal probability density functions. Upper limits on $\mathcal{B}_{H\to\text{inv}}$ are determined following the CL_s formalism [57] using the profile likelihood ratio as a test statistic.

3.1 Uncertainty correlation in Run 2 combination

In the combination of Run 2 results, most experimental systematic uncertainties, as well as the uncertainty on the integrated luminosity and the modelling of additional pp collisions in the same and neighbouring bunch crossings (pile-up), are correlated across all search channels. The assessment of some of the uncertainties associated with the calibration of the jet energy scale (JES) and the jet energy resolution varies between the different analyses in terms of jet reconstruction algorithms and parameterisation choices. For this reason, the uncertainty components stemming from identical methodologies are presumed to be correlated, while the rest of the uncertainties are treated as uncorrelated. Finally, a few experimental systematic uncertainties that are tightly constrained in a given analysis are not correlated in order not to introduce any potential phase space specific biases. The impact of these assumptions on the combined result is estimated by using alternative correlation models and found to have an absolute effect on the $\mathcal{B}_{H\to\text{inv}}$ limit of the order of 0.003.

The uncertainties related to background predictions are considered to be uncorrelated among analyses due to the different nature of the leading backgrounds, the variety of kinematic phase space covered by the various analyses, and the usage of data-driven techniques. The systematic uncertainties in the prediction of Higgs boson production follow the recommendations in Ref. [24]. Variations connected to the choice of parton distribution functions (PDF) are considered as correlated among channels while effects of missing higher-order contributions (estimates through variations of factorisation and renormalisation scales) and parton shower/hadronisation models are considered independently for each Higgs boson production mode and therefore uncorrelated across the analyses.

3.2 Uncertainty correlation in Run 1 and Run 2 combination

The Run 2 result described above is combined with the Run 1 searches for $H \to$ invisible decays. The adopted correlation scheme follows closely the statistical combination of the partial Run 2 results with the Run 1 combination [31].

The correlation schemes of the individual Run 1 and Run 2 combinations are preserved when combined together. Due to the differences between the detector layouts and data-taking conditions, reconstruction algorithms, which are calibrated using data, and treatment of systematic uncertainties, the correlations between the two LHC runs are not clearly identifiable. Hence, no correlations between Run 1 and 2 are assumed for most instrumental uncertainties. Exceptions are made for uncertainties related to the modelling of the calorimeter response dependence on jet flavour and pile-up, the calibration of the JES across different η regions, and the uncertainties related to the JES of b-quark jets. Such components are treated as correlated given that the same methodology was applied to compute them in both of the datasets.

Background modelling uncertainties are considered to be uncorrelated in order to reflect improvements in the MC simulation tools and general theory predictions that have evolved significantly since Run 1, both on the side of the hard process simulation and on the side of the parton shower and hadronisation models. For

similar reasons, the signal modelling uncertainties are considered uncorrelated between the Run 1 and Run 2 combinations.

The result of the combination shows little sensitivity to the exact correlation scheme between the Run 1 and Run 2 results due to the dominant weight of the latter.

4 Results

The value of twice the negative logarithmic profile likelihood ratio $-2 \ln(\Lambda)(\mathcal{B}_{H\to\text{inv}}; \theta)$ as a function of $\mathcal{B}_{H\to\text{inv}}$ of the individual analyses and of the combined Run 2 result are shown in Figure 2 (left). The combined best-fit value for $\mathcal{B}_{H\to\text{inv}}$ is 0.04 ± 0.04. Good agreement among the best fit values of the individual analyses, reported in Table 1, is observed.
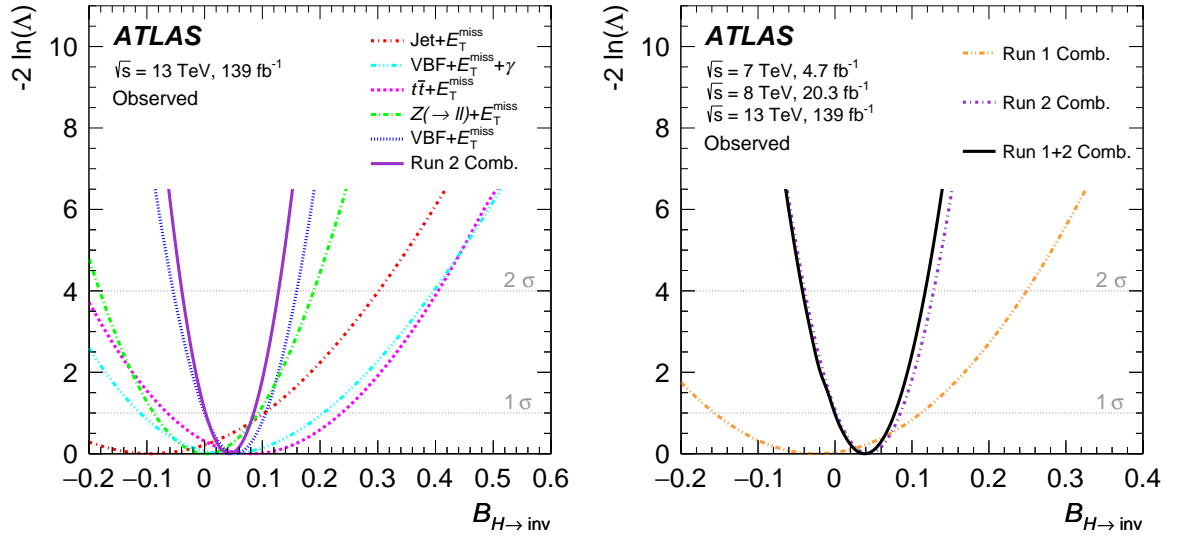

Figure 2: The observed value of $-2 \ln(\Lambda)$ as a function of $\mathcal{B}_{H\to\text{inv}}$ for the individual Run 2 analyses and their combination (left) and the Run 2 combination together with the Run 1 combination and the total Run 1+2 combination (right).

The best-fit values for $\mathcal{B}_{H\to\text{inv}}$ together with the 95% CL expected and observed upper limits for each individual Run 2 analysis and their combination are also shown in Table 1. An upper limit of 0.113 is observed for the combined Run 2 data, while an upper limit of 0.080 was expected in the case of no observed excess in data. Relative to the most sensitive single analysis, the VBF final state, the Run 2 combination brings a relative sensitivity improvement of 22%.

Overall, the leading systematic uncertainty of the result is due to the modelling uncertainties of the W/Z+jets prediction. Subdominant uncertainties with similar contribution are related to the statistical precision of the data sample; the number of simulated MC events, in particular for the W/Z+jets process; the reconstruction and identification of jets and leptons; and the modelling of background processes other than from W/Z+jets production.

Table 1: Best fit value, observed and expected 95% upper limit on $\mathcal{B}_{H\to\text{inv}}$ for each individual Run 2 analysis, their combination, the Run 1 combination and the full Run 1+2 combination.

Analysis	Best fit $\mathcal{B}_{H\to\text{inv}}$	Observed 95% U.L.	Expected 95% U.L.
Jet + $E_{\text{T}}^{\text{miss}}$	$-0.09^{+0.19}_{-0.20}$	0.329	$0.383^{+0.157}_{-0.107}$
VBF + $E_{\text{T}}^{\text{miss}}$ + γ	$0.04^{+0.17}_{-0.15}$	0.375	$0.346^{+0.151}_{-0.097}$
$t\bar{t}$ + $E_{\text{T}}^{\text{miss}}$	0.08 ± 0.15	0.376	$0.295^{+0.125}_{-0.083}$
$Z(\to \ell\ell)$ + $E_{\text{T}}^{\text{miss}}$	0.00 ± 0.09	0.185	$0.185^{+0.078}_{-0.052}$
VBF + $E_{\text{T}}^{\text{miss}}$	0.05 ± 0.05	0.145	$0.103^{+0.041}_{-0.028}$
Run 2 Comb.	0.04 ± 0.04	0.113	$0.080^{+0.031}_{-0.022}$
Run 1 Comb.	$-0.02^{+0.14}_{-0.13}$	0.252	$0.265^{+0.105}_{-0.074}$
Run 1+2 Comb.	0.04 ± 0.04	0.107	$0.077^{+0.030}_{-0.022}$

The observed $-2\ln(\Lambda)(\mathcal{B}_{H\to\text{inv}}; \theta)$ scan of the combined Run 1+2 result is represented in Figure 2 (right), alongside the individual Run 1 and Run 2 combinations. A best-fit value of $\mathcal{B}_{H\to\text{inv}} = 0.04 \pm 0.04$ is obtained for the Run 1+2 combination, corresponding to an observed (expected) upper limit of $\mathcal{B}_{H\to\text{inv}} < 0.107\ (0.077)$ at the 95% CL. The result is dominated by the Run 2 analysis with the addition of Run 1 combination improving the expected relative sensitivity by 4%.

The overall picture of the most relevant sources of uncertainty in the Run 1+Run 2 combination is very similar to that of the Run 2 combination and the upper limit would improve by 50% if all sources of systematic uncertainties were ignored.

The upper limits for each individual Run 2 analysis, their combination, the Run 1 combination and the overall Run 1+2 combined result are summarised in Figure 3. The current combination improves the constraints on $\mathcal{B}_{H\to\text{inv}}$ by more than a factor of two as compared to the previous ATLAS combination from Run 1 and partial Run 2 results [31].

5 Comparison to direct dark matter detection experiments

The combined observed Run 1+2 upper limit on $\mathcal{B}_{H\to\text{inv}}$ can be converted into a limit on the spin-independent scattering cross-section of a weakly interacting massive particle (WIMP) and a nucleon [13, 18, 58, 59], $\sigma_{\text{WIMP-Nucleon}}$. The translation is performed in the context of Higgs portal models [15, 60] using an effective field theory framework, where the mediator of new interactions is assumed to be above the TeV-level and therefore well above the scale probed at the Higgs boson mass. The approach assumes that Higgs boson decays into a pair of WIMP particles are kinematically possible ($m_{\text{WIMP}} < m_H/2$) and that the WIMP particle is either a scalar, a Majorana fermion, or a vector-like state[2]. In addition, in the case of vectorial DM states, various ultraviolet-complete (UV) models were proposed [62–64]. In such scenarios, the vector DM candidate is introduced as a gauge field of a U(1)′ group which extends the SM symmetry group and a dark Higgs sector is added to generate the vector boson mass via the Higgs

---

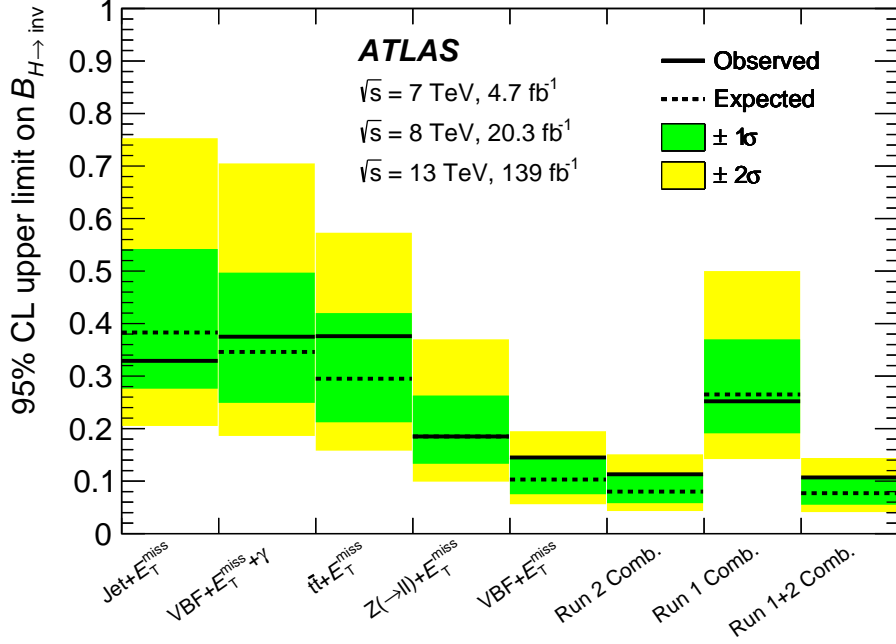[2] The value of $f_N = 0.308 \pm 0.018$ [61] is used as nuclear form factor.

Figure 3: The observed and expected upper limits on $\mathcal{B}_{H \to \text{inv}}$ at 95% CL for the Run 2 analyses targetting the Jet + E_T^{miss}, VBF + E_T^{miss} + γ, $t\bar{t}$ + E_T^{miss}, $Z(\to \ell\ell)$ + E_T^{miss}, VBF + E_T^{miss} final states and their combination, the Run 1 combination and the full Run 1+2 result; the 1σ and 2σ contours of the expected limit distribution are also shown.

spontaneous symmetry breaking mechanism. This adds at least two free parameters to the model: the mass m_2 of the additional dark Higgs boson and its mixing angle α with SM Higgs boson.

The constraint from the combined observed Run 1+2 exclusion limit of $\mathcal{B}_{H \to \text{inv}}$ < 0.093 at 90% CL is compared to the results from representative direct DM detection experiments [65–68] in Figure 4. The excluded $\sigma_{\text{WIMP-Nucleon}}$ values range from 10^{-45} cm^2 to 10^{-42} cm^2 in the scalar WIMP scenario. In the Majorana fermion WIMP case, the effective coupling is reduced by a factor m_H^2 [27], excluding cross-section values down to 2×10^{-47} cm^2 for low WIMP masses; $\sigma_{\text{WIMP-Nucleon}}$ values down to 10^{-54} cm^2 can be excluded for the vector WIMP hypothesis. For UV-complete models, Figure 4 also shows the upper limit cross-section behaviour for a mixing angle $\alpha = 0.2$ and for masses of the Dark Higgs particle equal to 65 GeV and 100 GeV corresponding to the worst and best limit for a scan of m_2 in the range [65, 1000] GeV [64]. This comparison illustrates the complementarity in coverage by the direct-detection experiments and the searches at colliders, such as the presented analysis.
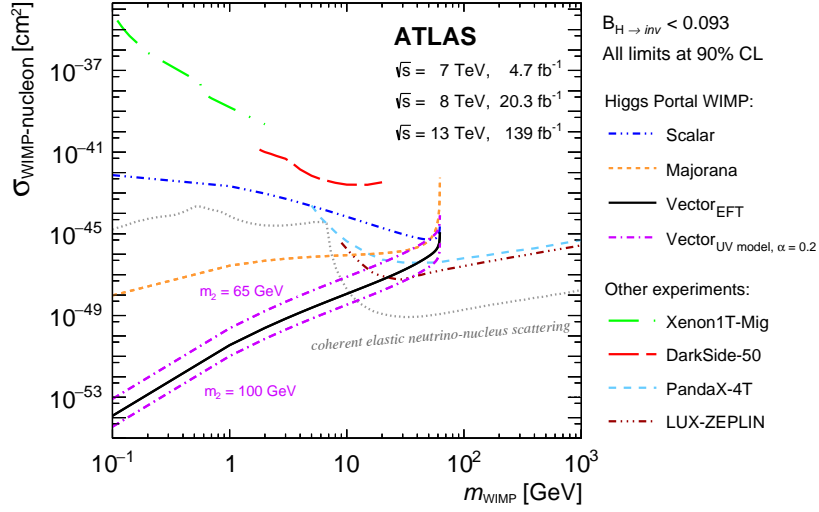
Figure 4: Upper limit at the 90% CL on the spin-independent WIMP-nucleon scattering cross-section as a function of the WIMP mass for direct detection experiments and the interpretation of the $H \rightarrow$ invisible combination result in the context of Higgs portal models considering scalar, Majorana and vector (WIMP hypotheses. For the vector case, results from UV-complete models are shown (pink curves) for two representative values for the mass of the predicted Dark Higgs particle (m_2) and a mixing angle α=0.2. The uncertainties from the nuclear form factor are smaller than the line thickness. Direct detection results are taken from Refs. [65–68]. The neutrino floor for coherent elastic neutrino-nucleus scattering (solid gray line) is taken from Refs. [69, 70], which assume that germanium is the target over the whole WIMP mass range. The regions above the limit contours are excluded in the range shown in the plot.

6 Conclusion

In summary, searches for invisible decays of the Higgs boson using 139 fb^{-1} of pp collision data at $\sqrt{s}$ = 13 TeV recorded in Run 2 of the LHC in several Higgs boson production topologies were statistically combined assuming SM Higgs boson production. An upper limit on the invisible Higgs boson branching ratio of $\mathcal{B}_{H \rightarrow \text{inv}} < 0.113$ ($0.080^{+0.031}_{-0.022}$) is observed (expected) at the 95% CL. A statistical combination of this result with the combination of $H \rightarrow$ invisible searches using up to 4.7 fb^{-1} of pp collision data at $\sqrt{s}$ = 7 TeV and up to 20.3 fb^{-1} at 8 TeV collected in Run 1 of the LHC yields an observed (expected) upper limit of $\mathcal{B}_{H \rightarrow \text{inv}} < 0.107$ ($0.077^{+0.030}_{-0.022}$) at the 95% CL. The combined Run 1+2 result is translated into upper limits on the WIMP-nucleon scattering cross-section for Higgs portal models. The derived limits on $\sigma_{\text{WIMP-Nucleon}}$ range down to 10^{-45} cm^2 (scalar), 2×10^{-47} cm^2 (Majorana) and 10^{-54} cm^2 (vector), highlighting the complementarity of DM searches at the LHC and direct detection experiments.

References

[1] F. Zwicky, *Die Rotverschiebung von extragalaktischen Nebeln*, Helv. Phys. Acta **6** (1933) 110.

[2] G. Bertone, D. Hooper and J. Silk, *Particle dark matter: Evidence, candidates and constraints*, Phys. Rept. **405** (2005) 279, arXiv: `hep-ph/0404175`.

[3] E. Komatsu et al., *SEVEN-YEAR WILKINSON MICROWAVE ANISOTROPY PROBE (WMAP) OBSERVATIONS: COSMOLOGICAL INTERPRETATION*, Astrophys. J. Suppl. **192** (2011) 18, arXiv: `1001.4538 [astro-ph.CO]`.

[4] Planck Collaboration, *Planck 2015 results. XIII. Cosmological parameters*, Astron. Astrophys. **594** (2016) A13, arXiv: 1502.01589 [astro-ph.CO].

[5] D. Abercrombie et al., *Dark Matter benchmark models for early LHC Run-2 Searches: Report of the ATLAS/CMS Dark Matter Forum*, Phys. Dark Univ. **27** (2020) 100371, arXiv: 1507.00966 [hep-ex].

[6] J. L. Feng, *Dark Matter Candidates from Particle Physics and Methods of Detection*, Annual Review of Astronomy and Astrophysics **48** (2010) 495, arXiv: 1003.0904 [astro-ph.CO].

[7] A. Boveia and C. Doglioni, *Dark Matter Searches at Colliders*, Annual Review of Nuclear and Particle Science **68** (2018) 429, arXiv: 1810.12238 [hep-ex].

[8] ATLAS Collaboration, *Observation of a new particle in the search for the Standard Model Higgs boson with the ATLAS detector at the LHC*, Phys. Lett. B **716** (2012) 1, arXiv: 1207.7214 [hep-ex].

[9] CMS Collaboration, *Observation of a new boson at a mass of 125 GeV with the CMS experiment at the LHC*, Phys. Lett. B **716** (2012) 30, arXiv: 1207.7235 [hep-ex].

[10] I. Antoniadis, M. Tuckmantel and F. Zwirner, *Phenomenology of a leptonic goldstino and invisible Higgs boson decays*, Nucl. Phys. **707** (2005) 215, arXiv: hep-ph/0410165 [hep-ph].

[11] N. Arkani-Hamed, S. Dimopoulos, G. R. Dvali and J. March-Russell, *Neutrino masses from large extra dimensions*, Phys. Rev. D **65** (2001) 024032, arXiv: hep-ph/9811448 [hep-ph].

[12] A. Datta, K. Huitu, J. Laamanen and B. Mukhopadhyaya, *Linear collider signals of an invisible Higgs boson in theories of large extra dimensions*, Phys. Rev. D **70** (2004) 075003, arXiv: hep-ph/0404056 [hep-ph].

[13] S. Kanemura, S. Matsumoto, T. Nabeshima and N. Okada, *Can WIMP dark matter overcome the nightmare scenario?*, Phys. Rev. D **82** (2010) 055026, arXiv: 1005.5651 [hep-ph].

[14] A. Djouadi, O. Lebedev, Y. Mambrini and J. Quevillon, *Implications of LHC searches for Higgs–portal dark matter*, Phys. Lett. B **709** (2012) 65, arXiv: 1112.3299 [hep-ph].

[15] A. Djouadi, A. Falkowski, Y. Mambrini and J. Quevillon, *Direct detection of Higgs-portal dark matter at the LHC*, Eur. Phys. J. C **73** (2013) 2455, arXiv: 1205.3169 [hep-ph].

[16] R. E. Shrock and M. Suzuki, *Invisible Decays of Higgs Bosons*, Phys. Lett. B **110** (1982) 250.

[17] D. Choudhury and D. P. Roy, *Signatures of an invisibly decaying Higgs particle at LHC*, Phys. Lett. B **322** (1994) 368, arXiv: hep-ph/9312347 [hep-ph].

[18] O. J. P. Eboli and D. Zeppenfeld, *Observing an invisible Higgs boson*, Phys. Lett. B **495** (2000) 147, arXiv: hep-ph/0009158 [hep-ph].

[19] H. Davoudiasl, T. Han and H. E. Logan, *Discovering an invisibly decaying Higgs boson at hadron colliders*, Phys. Rev. D **71** (2005) 115007, arXiv: hep-ph/0412269 [hep-ph].

[20] R. M. Godbole, M. Guchait, K. Mazumdar, S. Moretti and D. P. Roy,
Search for 'invisible' Higgs signals at LHC via associated production with gauge bosons,
Phys. Lett. B **571** (2003) 184, arXiv: `hep-ph/0304137 [hep-ph]`.

[21] D. Ghosh, R. Godbole, M. Guchait, K. Mohan and D. Sengupta,
Looking for an Invisible Higgs Signal at the LHC, Phys. Lett. B **725** (2013) 344,
arXiv: `1211.7015 [hep-ph]`.

[22] G. Belanger, B. Dumont, U. Ellwanger, J. F. Gunion and S. Kraml, *Status of invisible Higgs decays*,
Phys. Lett. B **723** (2013) 340, arXiv: `1302.5694 [hep-ph]`.

[23] D. Curtin et al., *Exotic decays of the 125 GeV Higgs boson*, Phys. Rev. D **90** (2014) 075004,
arXiv: `1312.4992 [hep-ph]`.

[24] D. de Florian et al.,
Handbook of LHC Higgs Cross Sections: 4. Deciphering the Nature of the Higgs Sector, (2016),
arXiv: `1610.07922 [hep-ph]`.

[25] ATLAS Collaboration, *The ATLAS Experiment at the CERN Large Hadron Collider*,
JINST **3** (2008) S08003.

[26] ATLAS Collaboration, *ATLAS Insertable B-Layer Technical Design Report*,
ATLAS-TDR-19; CERN-LHCC-2010-013, 2010,
URL: `https://cds.cern.ch/record/1291633`, Addendum: ATLAS-TDR-19-ADD-1;
CERN-LHCC-2012-009, 2012, URL: `https://cds.cern.ch/record/1451888`.

[27] ATLAS Collaboration, *Search for invisible decays of a Higgs boson using vector-boson fusion in pp collisions at $\sqrt{s} = 8\,TeV$ with the ATLAS detector*, JHEP **01** (2016) 172,
arXiv: `1508.07869 [hep-ex]`.

[28] ATLAS Collaboration,
Search for Invisible Decays of a Higgs Boson Produced in Association with a Z Boson in ATLAS,
Phys. Rev. Lett. **112** (2014) 201802, arXiv: `1402.3244 [hep-ex]`.

[29] ATLAS Collaboration, *Search for invisible decays of the Higgs boson produced in association with a hadronically decaying vector boson in pp collisions at $\sqrt{s} = 8\,TeV$ with the ATLAS detector*,
Eur. Phys. J. C **75** (2015) 337, arXiv: `1504.04324 [hep-ex]`.

[30] ATLAS Collaboration, *Constraints on new phenomena via Higgs boson couplings and invisible decays with the ATLAS detector*, JHEP **11** (2015) 206, arXiv: `1509.00672 [hep-ex]`.

[31] ATLAS Collaboration,
Combination of Searches for Invisible Higgs Boson Decays with the ATLAS Experiment,
Phys. Rev. Lett. **122** (2019) 231801, arXiv: `1904.05105 [hep-ex]`.

[32] CMS Collaboration, *Search for invisible decays of a Higgs boson produced through vector boson fusion in proton–proton collisions at $\sqrt{s} = 13\,TeV$*, Phys. Lett. B **793** (2019) 520,
arXiv: `1809.05937 [hep-ex]`.

[33] ATLAS Collaboration, *Search for invisible Higgs-boson decays in events with vector-boson fusion signatures using $139\,fb^{-1}$ of proton–proton data recorded by the ATLAS experiment*,
JHEP **08** (2022) 104, arXiv: `2202.07953 [hep-ex]`.

[34] ATLAS Collaboration, *Observation of electroweak production of two jets in association with an isolated photon and missing transverse momentum, and search for a Higgs boson decaying into invisible particles at 13 TeV with the ATLAS detector*, Eur. Phys. J. C **82** (2021) 105,
arXiv: `2109.00925 [hep-ex]`.

[35] ATLAS Collaboration, *Constraints on spin-0 dark matter mediators and invisible Higgs decays using ATLAS* 13 *TeV pp collision data with two top quarks and missing energy in the final state*, ATLAS-CONF-2022-007, 2022, URL: https://cds.cern.ch/record/2805211.

[36] ATLAS Collaboration, *Search for associated production of a Z boson with an invisibly decaying Higgs boson or dark matter candidates at $\sqrt{s} = 13$ TeV with the ATLAS detector*, Phys. Lett. B **829** (2021) 137066, arXiv: 2111.08372 [hep-ex].

[37] ATLAS Collaboration, *Search for new phenomena in events with an energetic jet and missing transverse momentum in pp collisions at $\sqrt{s} = 13$ TeV with the ATLAS detector*, Phys. Rev. D **103** (2021) 112006, arXiv: 2102.10874 [hep-ex].

[38] CMS Collaboration, *Search for dark matter produced in association with a leptonically decaying Z boson in proton–proton collisions at $\sqrt{s} = 13$ TeV*, Eur. Phys. J. C **81** (2021) 13, arXiv: 2008.04735 [hep-ex].

[39] CMS Collaboration, *Search for invisible decays of the Higgs boson produced via vector boson fusion in proton–proton collisions at $\sqrt{s} = 13$ TeV*, Phys. Rev. D **105** (2022) 092007, arXiv: 2201.11585 [hep-ex].

[40] CMS Collaboration, *Search for new particles in events with energetic jets and large missing transverse momentum in proton–proton collisions at $\sqrt{s} = 13$ TeV*, JHEP **11** (2021) 153, arXiv: 2107.13021 [hep-ex].

[41] ATLAS Collaboration, *A detailed map of Higgs boson interactions by the ATLAS experiment ten years after the discovery*, Nature **607** (2022) 52, arXiv: 2207.00092 [hep-ex].

[42] K. Kudashkin, J. M. Lindert, K. Melnikov and C. Wever, *Higgs bosons with large transverse momentum at the LHC*, Phys. Lett. B **782** (2018) 210, arXiv: 1801.08226 [hep-ph].

[43] A. Djouadi, J. Kalinowski, M. Mühlleitner and M. Spira, *HDECAY: Twenty++ years after*, Comput. Phys. Commun. **238** (2019) 214, arXiv: 1801.09506 [hep-ph].

[44] M. Bonetti, K. Melnikov and L. Tancredi, *Higher order corrections to mixed QCD-EW contributions to Higgs boson production in gluon fusion*, Phys. Rev. D **97** (2018) 056017, arXiv: 1801.10403 [hep-ph], Erratum: Phys. Rev. D **97** (2018) 099906.

[45] F. Dulat, A. Lazopoulos and B. Mistlberger, *iHixs 2 – Inclusive Higgs cross sections*, Comput. Phys. Commun. **233** (2018) 243, arXiv: 1802.00827 [hep-ph].

[46] R. V. Harlander, J. Klappert, S. Liebler and L. Simon, *vh@nnlo-v2: new physics in Higgs Strahlung*, JHEP **05** (2018) 089, arXiv: 1802.04817 [hep-ph].

[47] M. Cacciari, F. A. Dreyer, A. Karlberg, G. P. Salam and G. Zanderighi, *Fully Differential Vector-Boson-Fusion Higgs Production at Next-to-Next-to-Leading Order*, Phys. Rev. Lett. **115** (2015) 082002, arXiv: 1506.02660 [hep-ph], Erratum: Phys. Rev. Lett. **120** (2018) 139901.

[48] ATLAS Collaboration, *Constraints on spin-0 dark matter mediators and invisible Higgs decays using ATLAS 13 TeV pp collision data with two top quarks and missing transverse momentum in the final state*, 2022, arXiv: 2211.05426 [hep-ex].

[49] ATLAS Collaboration, *ATLAS b-jet identification performance and efficiency measurement with $t\bar{t}$ events in pp collisions at $\sqrt{s}$ = 13 TeV*, Eur. Phys. J. C **79** (2019) 970, arXiv: 1907.05120 [hep-ex].

[50] J. M. Lindert, S. Pozzorini and M. Schönherr, *Precise predictions for V+2 jet backgrounds in searches for invisible Higgs decays*, 2022, arXiv: 2204.07652 [hep-ph].

[51] ATLAS Collaboration, *Search for a scalar partner of the top quark in the all-hadronic $t\bar{t}$ plus missing transverse momentum final state at $\sqrt{s}$ = 13 TeV with the ATLAS detector*, Eur. Phys. J. C **80** (2020) 737, arXiv: 2004.14060 [hep-ex].

[52] ATLAS Collaboration, *Search for new phenomena with top quark pairs in final states with one lepton, jets, and missing transverse momentum in pp collisions at $\sqrt{s}$ = 13 TeV with the ATLAS detector*, JHEP **04** (2020) 174, arXiv: 2012.03799 [hep-ex].

[53] ATLAS Collaboration, *Search for new phenomena in events with two opposite-charge leptons, jets and missing transverse momentum in pp collisions at $\sqrt{s}$ = 13 TeV with the ATLAS detector*, JHEP **04** (2021) 165, arXiv: 2102.01444 [hep-ex].

[54] G. Cowan, K. Cranmer, E. Gross and O. Vitells, *Asymptotic formulae for likelihood-based tests of new physics*, Eur. Phys. J. C **71** (2011) 1554, arXiv: 1007.1727 [physics.data-an], Erratum: Eur. Phys. J. C **73** (2013) 2501.

[55] W. Verkerke and D. Kirkby, *The RooFit toolkit for data modeling*, 2003, arXiv: physics/0306116 [physics.data-an].

[56] L. Moneta et al., *The RooStats project*, PoS **ACAT2010** (2010) 057, arXiv: 1009.1003 [physics.data-an].

[57] A. L. Read, *Presentation of search results: the CL_S technique*, J. Phys. G **28** (2002) 2693.

[58] P. J. Fox, R. Harnik, J. Kopp and Y. Tsai, *Missing energy signatures of dark matter at the LHC*, Physical Review D **85** (2012), ISSN: 1550-2368, arXiv: 1109.4398.

[59] A. De Simone, G. F. Giudice and A. Strumia, *Benchmarks for dark matter searches at the LHC*, JHEP **06** (2014) 081, arXiv: 1402.6287.

[60] B. Patt and F. Wilczek, *Higgs-field portal into hidden sectors*, 2006, arXiv: hep-ph/0605188 [hep-ph].

[61] M. Hoferichter, P. Klos, J. Menéndez and A. Schwenk, *Improved Limits for Higgs-Portal Dark Matter from LHC Searches*, Phys. Rev. Lett. **119** (2017) 181803, arXiv: 1708.02245 [hep-ph].

[62] S. Baek, P. Ko and W.-I. Park, *Invisible Higgs decay width versus dark matter direct detection cross section in Higgs portal dark matter models*, Phys. Rev. D **90** (2014) 055014, arXiv: 1405.3530 [hep-ph].

[63] G. Arcadi, A. Djouadi and M. Kado, *The Higgs-portal for vector Dark Matter and the Effective Field Theory approach: a reappraisal*, Phys. Lett. B **805** (2020) 135427, arXiv: 2001.10750 [hep-ph].

[64] M. Zaazoua, L. Truong, K. A. Assamagan and F. Fassi, *Higgs Portal Vector Dark Matter Interpretation: Review of Effective Field Theory Approach and Ultraviolet Complete Models*, Letters in High Energy Physics (2022) 270, arXiv: 2107.01252 [hep-ph].

[65] P. Agnes et al., *Low-Mass Dark Matter Search with the DarkSide-50 Experiment*, Physical Review Letters **121** (2018), arXiv: 1802.06994.

[66] Y. Meng et al., *Dark Matter Search Results from the PandaX-4T Commissioning Run*, Physical Review Letters **127** (2021), arXiv: 2107.13438.

[67] J. Aalbers et al., *First Dark Matter Search Results from the LUX-ZEPLIN (LZ) Experiment*, (2022), arXiv: 2207.03764 [hep-ex].

[68] E. Aprile et al., *Search for Light Dark Matter Interactions Enhanced by the Migdal Effect or Bremsstrahlung in XENON1T*, Phys. Rev. Lett. **123** (2019) 241803, arXiv: 1907.12771 [hep-ex].

[69] J. Billard, E. Figueroa-Feliciano and L. Strigari, *Implication of neutrino backgrounds on the reach of next generation dark matter direct detection experiments*, Physical Review D **89** (2014), arXiv: 1307.5458 [hep-ph].

[70] F. Ruppin, J. Billard, E. Figueroa-Feliciano and L. Strigari, *Complementarity of dark matter detectors in light of the neutrino background*, Physical Review D **90** (2014), arXiv: 1408.3581.